

Natural Multicontact Walking for Robotic Assistive Devices via Musculoskeletal Models and Hybrid Zero Dynamics

Kejun Li¹, Maegan Tucker², Rachel Gehlhar², Yisong Yue¹, and Aaron D. Ames^{1,2}

Abstract—Generating provably stable walking gaits that yield natural locomotion when executed on robotic-assistive devices is a challenging task that often requires hand-tuning by domain experts. This paper presents an alternative methodology, where we propose the addition of musculoskeletal models directly into the gait generation process to intuitively shape the resulting behavior. In particular, we construct a multi-domain hybrid system model that combines the system dynamics with muscle models to represent natural multicontact walking. Stable walking gaits can then be formally generated for this model via the hybrid zero dynamics method. We experimentally apply our framework towards achieving multicontact locomotion on a dual-actuated transfemoral prosthesis, AMPRO3. The results demonstrate that enforcing feasible muscle dynamics produces gaits that yield natural locomotion (as analyzed via electromyography), without the need for extensive manual tuning. Moreover, these gaits yield similar behavior to expert-tuned gaits. We conclude that the novel approach of combining robotic walking methods (specifically HZD) with muscle models successfully generates anthropomorphic robotic-assisted locomotion.

I. INTRODUCTION

While there is extensive literature on the biomechanics surrounding non-disabled human walking [1], it is poorly understood how to translate this natural and efficient bipedal locomotion to robotic platforms, especially in the context of robotic assistive devices which necessitate cooperation with human users. In this work, we aim to achieve stable and natural assisted locomotion, without the need for extensive domain-expert tuning, by incorporating musculoskeletal models directly into a multi-domain gait generation process.

Even though bipedal locomotion is seemingly effortless for humans, achieving stable walking on robotic platforms is challenging as it requires accounting for discrete impact events, underactuation, and complicated nonlinear dynamics. Existing methods that have successfully demonstrated stable robotic locomotion include reduced-order models [2]–[5], formal model-based gait generation [6], [7], and reinforcement learning [8], [9]. Of these approaches, we are particularly interested in the *Hybrid Zero Dynamics* (HZD) method [10], [11], which is a mathematical approach leveraging the hybrid system model of locomotion, and capable of synthesizing provably stable [12] dynamic walking gaits on bipedal robots, encoded by impact-invariant periodic orbits. This method has been demonstrated on a number of robotic

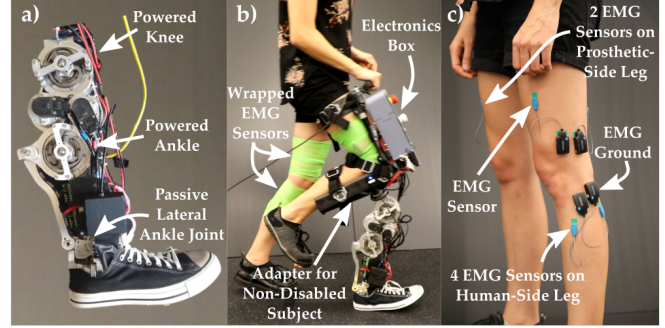


Fig. 1: a) AMPRO3 prosthesis, b) Non-disabled subject wearing the device during multicontact locomotion, c) placement of the surface mount electrodes for electromyography (EMG).

platforms and behaviors [13]–[15], including dynamic multicontact walking on 3D robots [16].

While the HZD method yields provably stable walking, one drawback of the approach is the reliance on a carefully-tuned optimization problem to obtain converged solutions for stable period orbits. For new applications, this tuning process usually entails weeks, if not months, of domain-expert tuning (typically involving modifying the cost and constraints until “good” gaits are found). This is especially problematic for robotic assistive devices since they require not only stable but also natural locomotion to alleviate high energy expenditure during ambulation, which demands even more hand-tuning to sufficiently constraint the problem.

Other existing approaches towards realizing natural walking include incorporating human walking data [17], [18], learning from experimental metrics such as electromyography (EMG) signals and metabolic expenditure [19], [20], and controlling devices using musculoskeletal models [21], [22]. However, these methods either lack stability guarantees or are data-driven, whereby the performance heavily relies on the quality and quantity of the data. Moreover, such data is behavior-specific and not always accessible.

In this work, we present an alternative approach based upon hybrid system models of locomotion that utilize musculoskeletal models — to our best knowledge, this is the first time these two modeling paradigms have been combined. Our proposed framework both enjoys the theoretical guarantees of stability via the HZD method, while also achieving natural locomotion without excessive tuning. Since humans usually self-select gaits that are physiologically and mechanically energy efficient [23], we hypothesize that generating stable gaits that satisfy muscle dynamics would naturally lead to more anthropomorphic and efficient behavior that respects physiological limits.

This research was supported by NSF GRF No. DGE-1745301, Wandercraft, and the ZEITLIN Fund, and conducted under IRB No. 16-0693.

¹Authors are with the Department of Computing and Mathematical Sciences, California Institute of Technology, Pasadena, CA 91125

²Authors are with the Department of Mechanical and Civil Engineering, California Institute of Technology, Pasadena, CA 91125

This hypothesis will be evaluated throughout this paper by first generating multicontact walking gaits utilizing HZD coupled with musculoskeletal models, followed by the experimental implementation on a dual-actuated transfemoral prosthesis, AMPRO3, shown in Fig. 1. The experimental results demonstrate that the novel combination of musculoskeletal models with HZD results in natural multicontact locomotion, as demonstrated in practice and quantified via electromyography (EMG).

II. MUSCLE MODEL

In this section, we introduce how a single muscle-tendon unit (MTU) is modeled. Later, in Sec. IV, we will provide details on how we extend these muscle models to multiple muscles and incorporate them into the Hybrid Zero Dynamics (HZD) gait generation framework.

Muscle-tendon Unit (MTU). We model each muscle as a two-element Hill-type muscle-tendon unit [24] with a contractile element (CE) and a series elastic element (SE) as shown in Fig. 2, similar to the model used in [25]. The constant parameters of each muscle are defined in [25], [26].

MTU Length. The length of an individual MTU, denoted by $l_{mtu} \in \mathbb{R}$, is modeled as $l_{mtu} = l_{se} + l_{ce}$, where $l_{ce} \in \mathbb{R}$ is the length of the contractile element (CE), and $l_{se} \in \mathbb{R}$ is the length of the series elasticity element (SE). Since the relative change of l_{mtu} depends on the individual joint angle $\theta \in \mathbb{R}$, with the collection of d joint angles denoted $q \in \mathbb{R}^d$, in practice we model the MTU length as a function of q :

$$l_{mtu}(q) = l_{opt} + l_{slack} - \sum_{j=1}^{j_N} \Delta l_{mtu}(\theta_j),$$

where $l_{opt}, l_{slack} \in \mathbb{R}$ are reference length of CE and SE, respectively, at reference angle $\theta_{ref} \in \mathbb{R}$. We use $\sum_{j=1}^{j_N} \Delta l_{mtu}(\theta_j)$ to denote the total change in length of the MTU based on the joint angles of each joint spanned by the MTU, out of a total of $j_N \in \{1, 2\}$ joints. The joints spanned by each MTU are illustrated in Fig.3a. The individual change in length due to a single joint, $\Delta l_{mtu}(\theta) \in \mathbb{R}$, is given by:

$$\Delta l_{mtu}(\theta) = \begin{cases} \rho r(\theta - \theta_{ref}), & \text{for hip} \\ \rho r[\sin(\theta - \theta_{max}) - \sin(\theta_{ref} - \theta_{max})], & \text{otherwise} \end{cases}$$

The constant $\rho \in \mathbb{R}$ is a parameter that ensures the fiber length is within the physiological limits and accounts for muscle pennation angles (the angle between the longitudinal axis of the entire muscle and its fibers that increases as the tension increases in the muscle). For the MTUs that span two joints, $\Delta l_{mtu}(\theta)$ is calculated separately with different reference angles θ_{ref} for each joint.

MTU Force-Length and Force-Velocity Relationships. The velocity of the CE contraction is denoted by $v_{ce} \in \mathbb{R}$ and is constrained to satisfy the relationship $l_{ce} = \int v_{ce} dt$. Depending on an MTU's instantaneous value of l_{ce} and v_{ce} , the amount of force the MTU is capable of exerting

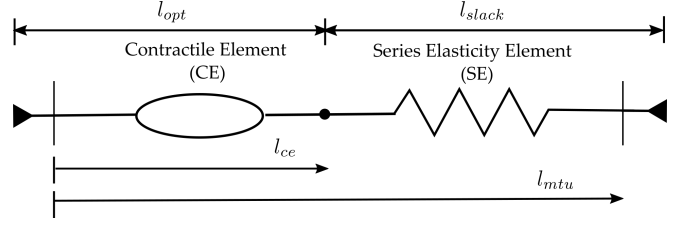


Fig. 2: A single muscle tendon unit (MTU) consists of a contractile element (CE) and a series elasticity element (SE). The length of CE and SE is denoted by l_{ce} and l_{se} . At the reference angle (θ_{ref}), the length of CE and SE is equal to l_{opt} and l_{slack} , respectively.

differs. This is described by the following force-length (f_l) and force-velocity (f_v) relationships:

$$f_l(l_{ce}) = \exp\left(\log(c) \left| \frac{l_{ce} - l_{opt}}{l_{opt}w} \right|^3\right),$$

$$f_v(v_{ce}) = \begin{cases} \frac{v_{max} - v_{ce}}{v_{max} + K v_{ce}}, & \text{if } v_{ce} < 0 \\ N + \frac{(N-1)(v_{max} + v_{ce})}{7.56K v_{ce} - v_{max}}, & \text{if } v_{ce} \geq 0 \end{cases}$$

where $N, v_{max}, w, K \in \mathbb{R}$ are all muscle-dependent constants. Specifically, N is the eccentric force enhancement (modeling the increase in muscle force during active stretch), v_{max} is the maximum contractile velocity, and w and K are parameters that shape the force-length and force-velocity curves, respectively.

Similarly, the MTU force also depends on l_{se} . This is modeled using an additional force-length relationship:

$$f_{se}(l_{se}) = \begin{cases} \left(\frac{l_{se} - l_{slack}}{l_{slack}(\varepsilon_{ref})} \right)^2, & \text{if } l_{se} \geq l_{slack} \\ 0, & \text{otherwise} \end{cases}$$

where the $\varepsilon_{ref} \in \mathbb{R}$ is a constant parameter denoting the MTU strain when $f_{se}(l_{se}) = 1$. Note that in the actual implementation, we used a continuous function, fitted via least squares regression, to replace the piece-wise functions for f_{se} and f_v since continuous functions are required for the implementation of a nonlinear optimization program.

MTU Force. Because the SE and CE are in series, we model their respective forces, $F_{se} \in \mathbb{R}$ and $F_{ce} \in \mathbb{R}$, as equal to the total force exerted by the MTU, denoted by $F_m \in \mathbb{R}$. Explicitly, we enforce $F_m = F_{se} = F_{ce}$. We independently model the individual element forces as depending on the previously defined force-length and force-velocity relationships:

$$F_{ce}(l_{ce}, v_{ce}, s) = s F_{max} f_l(l_{ce}) f_v(v_{ce}),$$

$$F_{se}(l_{se}) = F_{max} f_{se}(l_{se}),$$

where $s \in [0, 1]$ is the activation level of the muscles, and $F_{max} \in \mathbb{R}$ is a constant parameter dictating the maximum allowable force of the MTU. Note that we assume muscle activation to be instantaneous.

MTU Force-Torque Relationship. The torque provided by the MTU, denoted by $u_m \in \mathbb{R}$, is calculated individually for

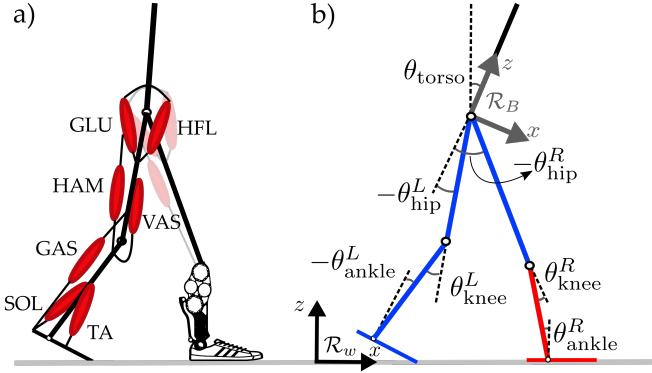


Fig. 3: a) Human-prosthesis system with the following seven labeled muscles on the intact leg: gluteus (GLU), hamstrings (HAM), gastrocnemius (GAS), soleus (SOL), hip flexors (HFL), and vastus (VAS), and tibialis anterior (TA). Three muscles (GLU, HAM, HFL) are also considered on the prosthetic leg side. b) Illustration of system coordinates, including the base and world frames.

each joint it spans using the following equations:

$$u_m = r(\theta) F_m, \quad (1)$$

$$r(\theta) = \begin{cases} r_0, & \text{for hip} \\ r_0 \cos(\theta - \theta_{max}), & \text{otherwise} \end{cases} \quad (2)$$

where $r(\theta) \in \mathbb{R}$ is the length of the MTU lever-arm, $r_0 \in \mathbb{R}$ is a parameter denoting the constant lever contribution, and $\theta_{max} \in \mathbb{R}$ is the reference angle at maximum lever contribution. For MTUs that span two joints, the muscle torque of each joint is calculated using different muscle-specific maximum lever contribution reference angles.

III. GENERATING MULTI-DOMAIN WALKING GAITS VIA THE HYBRID ZERO DYNAMICS METHOD

Next, we present a high-level introduction of the HZD method (without the inclusion of muscle models) applied to the AMPRO3 prosthesis. For more details, we refer the reader to [27], [28]. Additionally, information on the mechanical design of AMPRO3 is outlined in [29].

Human-Prosthesis Model for AMPRO3. The human-prosthesis system is modeled as a seven-link model, illustrated in Fig. 3b, with anthropomorphic parameters for the human segments (shown in blue), and parameters specific to the AMPRO3 prosthesis for the prosthetic segments (shown in red). Since the human user considered in this paper is not amputated, the model is asymmetric, with the knee of the prosthesis necessarily lower than the human knee.

The configuration space of the AMPRO3 prosthesis, assuming a floating-base convention [30], is defined as $\mathcal{Q} \subset \mathbb{R}^n$, where $n = 9$ is the planar unconstrained degrees of freedom of AMPRO3. We assume that the right leg is the intact leg and the left leg is the prosthetic leg. Hence, the human coordinates $q_h = (q_B^T, \theta_{hip}^L, \theta_{knee}^L, \theta_{ankle}^L, \theta_{hip}^R)^T$ consist of the base frame of the system and the joint angles of the human leg segments (left leg segments and right leg hip). The base frame is defined as $q_B = (p, \theta_{torso}) \in SE(2)$ with $p \in \mathbb{R}^2$ and $\theta_{torso} \in SO(2)$ being the position and rotation of the floating base frame R_B with respect to the world frame R_w . The prosthetic coordinates $q_p = (\theta_{knee}^R, \theta_{ankle}^R)^T$ include

the joint angles for the prosthetic segments. The generalized coordinate of the system is then defined as $q = (q_h^T, q_p^T)^T$ and the state space as $\mathcal{X} = T\mathcal{Q} \subset \mathbb{R}^{18}$ with coordinates $x = (q^T, \dot{q}^T)^T$.

Multi-Domain Hybrid System. To capture the intrinsic nature of human walking, a multi-domain hybrid system is constructed for the human-prosthesis system model, with the goal of matching the temporal domain pattern observed in natural human walking [31]. As illustrated in Fig. 4, we construct a domain pattern with eight distinct domains (four in each step), and eight transitions between domains. Note that since our model is asymmetric, we need to consider an entire gait cycle from right heel strike to the next right heel strike, consisting of two individual steps. The domains within each step are named according to the contact points as: Double Support 2 (DS2_{L,R}), Double Support 3 (DS3_{L,R}), Single Support 2 (SS2_{L,R}), and Single Support 1 (SS1_{L,R}), where the subscript $\{L, R\}$ denotes either the left or right stance leg step. These domains are similar to the breakdown in [16].

Equipped with the domain definitions, we construct a directed cycle $\Gamma = (V, E)$ to describe our multi-domain hybrid system, with the vertices $V = \{v_1, \dots, v_8\}$ and edges $E = \{e_1, \dots, e_8\}$ illustrated in Fig. 4. We denote the set of admissible domains by $\mathcal{D} = \{\mathcal{D}_v\}_{v \in V}$. The transitions between these domains are triggered by the set of guards, $S = \{S_e\}_{e \in E}$. The discrete dynamics of these transition events are denoted by $\Delta = \{\Delta_e\}_{e \in E}$.

We can then formally define our full hybrid system as a tuple $\mathcal{H} = (\Gamma, \mathcal{D}, \mathcal{U}, S, \Delta, FG)$, where $\mathcal{U} = \{\mathcal{U}_v\}_{v \in V}$ is the set of admissible inputs and $FG = \{(f_v, g_v)\}_{v \in V}$ is the set of control systems where (f_v, g_v) defines the *closed-loop continuous dynamics* $\dot{x} = f_{cl,v}(x) = f_v(x) + g_v(x) u_v$. For each domain, the system torque is defined as $u_v = [u_{hip}^L, u_{knee}^L, u_{ankle}^L, u_{hip}^R, u_{knee}^R, u_{ankle}^R]^T$. Lastly, the continuous dynamics can be obtained using the Euler-Lagrangian equation as explained in [28].

Virtual Constraints. The behavior of the hybrid system can be shaped using *virtual constraints*, which are defined as the difference between the actual system outputs $y^a(q)$ and the desired outputs $y^d(q, \alpha)$. In our work, we choose to describe the desired outputs using domain-specific Bézier polynomials with coefficients α_v . For non-underactuated domains (DS2, DS3, SS2), a relative degree one output is explicitly included in the virtual constraints in order to regulate the forward progression of the system:

$$y_v(q, \alpha) = \begin{bmatrix} y_{1,v}(q, \dot{q}, \alpha) \\ y_{2,v}(q, \alpha) \end{bmatrix} = \begin{bmatrix} y_{1,v}^a(q, \dot{q}) - v_{hip} \\ y_{2,v}^a(q) - y_{2,v}^d(\tau(q), \alpha) \end{bmatrix},$$

Here $y_{1,v} \in \mathbb{R}$ denotes the domain-specific relative degree one output, defined as the difference between the actual hip velocity $y_{1,v}^a(q, \dot{q})$ and the desired hip velocity v_{hip} . The remaining virtual constraints, $y_{2,v}(q, \alpha)$, denote the relative degree two virtual constraints. Since the linearized forward hip velocity, denoted by $\delta_{p_{hip}}(q)$, is approximately constant during the progress of each step cycle, we define our phase variable $\tau(q)$ as $\tau(q) = \frac{\delta_{p_{hip}}(q) - \delta_{p_{hip}}^+}{v_{hip}}$, where $\delta_{p_{hip}}^+$ is the

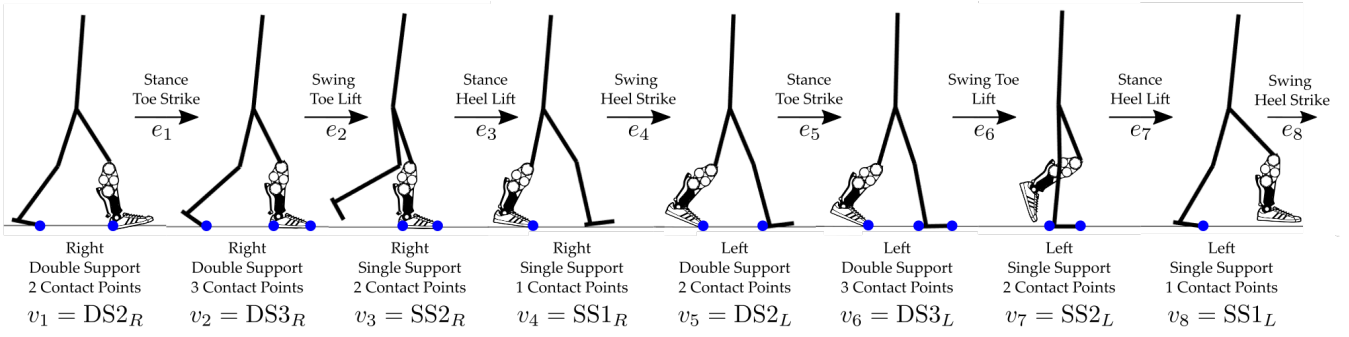


Fig. 4: A complete gait cycle from right heel strike to right heel strike. The gait cycle is described using the directed cycle $\Gamma = (V, E)$ with the vertices $V = \{v_1, \dots, v_8\}$ and edges $E = \{e_1, \dots, e_8\}$ illustrated in the figure. The naming convention is based on the stance leg of the step and the number of contact points. If both legs are in contact, the domain is considered as a double support domain.

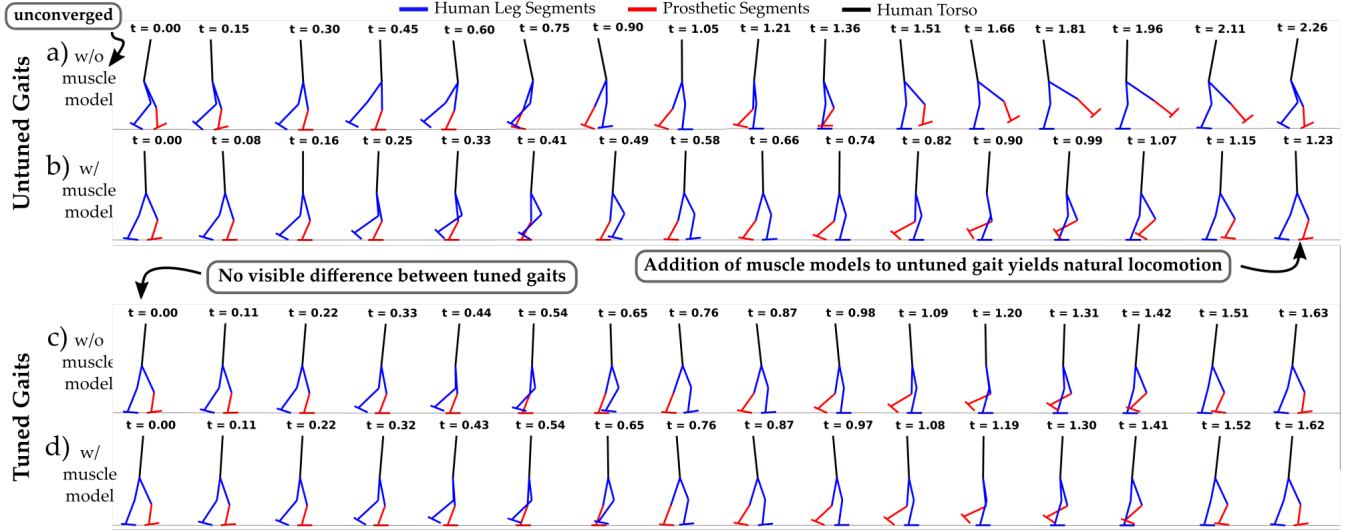


Fig. 5: Illustration of the generated gaits for a) untuned optimization without muscle models, b) untuned optimization with muscles, c) the tuned optimization without muscles, and d) the tuned optimization with muscles. The addition of the muscle model significantly changed the outcome of the untuned optimization problem, highlighting its ability to intuitively shape the generated walking behavior without the need for manually-added optimization constraints and tighter bounds. Furthermore the tuned gaits are nearly identical, illustrating the dominance of tight bounds/constraints on dictating the resulting behavior.

hip position at the beginning of the step. We select the virtual constraints for each domain within one step to be the following outputs:

$$\begin{aligned} y_{DS2} &= [v_{\text{hip}}, \theta_{\text{hip}}^{\text{st}}, \theta_{\text{knee}}^{\text{st}}, \theta_{\text{ankle}}^{\text{st}}, \theta_{\text{hip}}^{\text{sw}}, \theta_{\text{knee}}^{\text{sw}}]^T \\ y_{DS3} &= [v_{\text{hip}}, \theta_{\text{hip}}^{\text{st}}, \theta_{\text{knee}}^{\text{st}}, \theta_{\text{hip}}^{\text{sw}}, \theta_{\text{knee}}^{\text{sw}}]^T \\ y_{SS2} &= [v_{\text{hip}}, \theta_{\text{hip}}^{\text{st}}, \theta_{\text{knee}}^{\text{st}}, \theta_{\text{hip}}^{\text{sw}}, \theta_{\text{knee}}^{\text{sw}}, \theta_{\text{ankle}}^{\text{sw}}]^T \\ y_{SS1} &= [\theta_{\text{hip}}^{\text{st}}, \theta_{\text{knee}}^{\text{st}}, \theta_{\text{ankle}}^{\text{st}}, \theta_{\text{hip}}^{\text{sw}}, \theta_{\text{knee}}^{\text{sw}}, \theta_{\text{ankle}}^{\text{sw}}]^T \end{aligned}$$

where the superscripts (st, sw) denote either left (L) or right (R) for the stance and swing leg of the corresponding step. Note that the number of virtual constraints in each domain is dependent on the number of contact points.

Impact-Invariance Condition. While the continuous dynamics of the designed trajectory may be stable, the system can destabilize at impact events. Thus, it remains to construct desired trajectories that are *impact-invariant*. Since our hybrid system is a multi-domain system with both fully-actuated and under-actuated domains, the entire system is impact invariant if the following individual *impact-invariance*

conditions are met for each transition:

$$\begin{cases} \Delta_e(S_e \cap \mathcal{Z}_{\alpha_v}) \subseteq \mathcal{PZ}_{\alpha_v}, & e = \{3, 7\}, \\ \Delta_e(S_e \cap \mathcal{PZ}_{\alpha_v}) \subseteq \mathcal{Z}_{\alpha_v}, & e = \{4, 8\}, \\ \Delta_e(S_e \cap \mathcal{Z}_{\alpha_v}) \subseteq \mathcal{Z}_{\alpha_v}, & \text{otherwise.} \end{cases}$$

Here we use \mathcal{PZ}_{α_v} and \mathcal{Z}_{α_v} to denote the partial hybrid zero dynamics (PHZD) surface and HZD surface respectively:

$$\begin{aligned} \mathcal{Z}_{\alpha_v} &= \{(q, \dot{q}) \in \mathcal{D}_v : y_v(q, \alpha_v) = 0, \dot{y}_v(q, \dot{q}, \alpha_v) = 0\}, \\ \mathcal{PZ}_{\alpha_v} &= \{(q, \dot{q}) \in \mathcal{D}_v : y_{2,v}(q, \alpha_v) = 0, \dot{y}_{2,v}(q, \dot{q}, \alpha_v) = 0\}. \end{aligned}$$

The system evolves on these surfaces when the virtual constraints are driven to zero. Note that \mathcal{PZ}_{α_v} is a restriction of \mathcal{Z}_{α_v} for fully-actuated domains, in which the relative degree one output is used to regulate the system. In practice, impact-invariant periodic orbits are synthesized as solutions to a nonlinear optimization problem with constraints on the closed-loop dynamics and impact-invariance conditions.

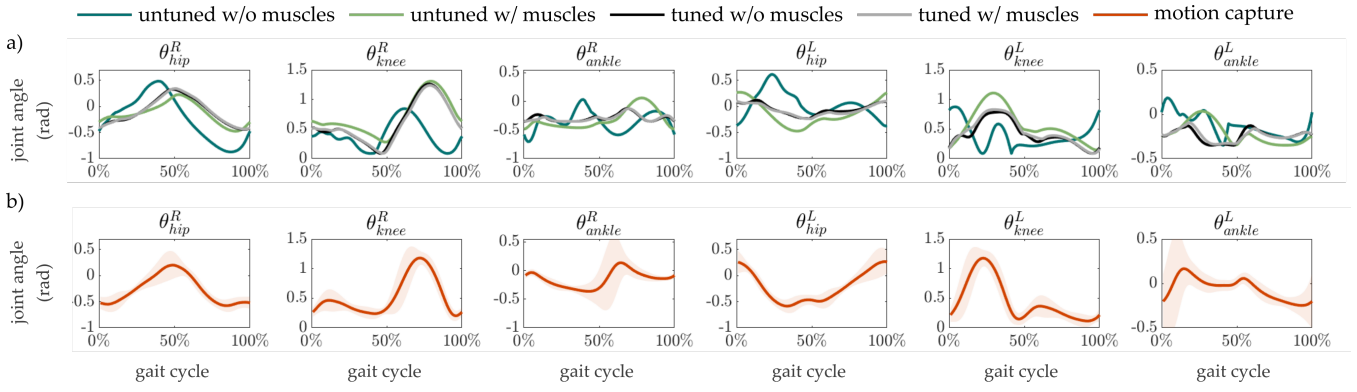


Fig. 6: Joint trajectories of the generated gaits (complete cycle from DS2_R to DS2_R). a) The joint trajectories for the tuned and untuned optimization problems with or without the muscle model. b) The joint trajectories for motion capture data of normal walking from [32].

IV. INTEGRATED FRAMEWORK WITH MUSCLE MODELS

To generate stable impact-invariant periodic orbits, with the inclusion of the muscle models presented in Sec. II, we construct a nonlinear optimization problem of the form:

$$\begin{aligned} \{\alpha^*, X^*\} = \underset{\alpha, X}{\operatorname{argmin}} \quad & \Phi_{\text{mCoT}}(X) \\ \text{s.t.} \quad & \text{C1.} \quad (\text{Closed-loop Dynamics}) \\ & \text{C2.} \quad (\text{Impact-Invariance Conditions}) \\ & \text{C3.} \quad (\text{Decision Variables}) \\ & \text{C4.} \quad (\text{Physical Constraints}) \\ & \text{C5-C12.} \quad (\text{Muscle Model Constraints}) \end{aligned}$$

where $\alpha = \{\alpha_v \mid v = 1, \dots, 8\}$ is our collection of Bézier coefficients for each domain, and X is the collection of all decision variables. We select our objective function to be the mechanical cost of transport (mCoT), $\Phi_{\text{mCoT}} = \int \frac{P(t)}{mgv} dt$, as defined in [16], since prior work has found it to yield natural and efficient locomotion [33].

Optimization Constraints. The first four constraints (C1-C4) of our framework are standard to the HZD method. The remaining constraints (C5-C12) enforce the muscle dynamics presented in Sec. II, and are explicitly defined as:

Muscle Model Constraints:

$$\begin{aligned} \text{C5. } \{F_m^{(i)} = F_{ce}^{(i)}(l_{ce}^{(i)}, v_{ce}^{(i)}, l_{se}^{(i)}, s^{(i)}), \forall i = 1, \dots, 10\} \\ \text{C6. } \{F_m^{(i)} = F_{se}(l_{se}^{(i)}), \forall i = 1, \dots, 10\} \\ \text{C7. } \{l_{ce}^{(i)} + l_{se}^{(i)} = l_{mtu}(q)^{(i)}, \forall i = 1, \dots, 10\} \\ \text{C8. } \{l_{ce}^{(i)} = \int v_{ce}^{(i)} dt, \forall i = 1, \dots, 10\} \\ \text{C9. } u_{hip}^L = u_m^{(1h)} + u_m^{(2)} + u_m^{(3)} \\ \text{C10. } u_{knee}^L = u_m^{(1k)} + u_m^{(4k)} - u_m^{(5)} \\ \text{C11. } u_{ankle}^L = u_m^{(4a)} + u_m^{(6)} - u_m^{(7)} \\ \text{C12. } u_{hip}^R = u_m^8 + u_m^9 - u_m^{10} \end{aligned}$$

where $i = 1, \dots, 10$ denotes a specific muscle out of the ten muscles we consider, illustrated in Fig. 3. These muscles consist of seven muscles on the intact leg (hamstring (HAM), glutes (GLU), hip flexor (HFL), gastrocnemius (GAS), vastus (VAS), soleus (SOL), tibialis anterior (TA)), and three muscles on the prosthetic leg (HAM, GLU, HFL).

	Converg. Status	Num. Iterations	Time (min)	Final Obj. Value
Untuned without muscles	0	10000	≈ 592	$\approx 1.58e^3$
Untuned with muscles	1	1793	≈ 32	$\approx 5.27e^{-4}$
Tuned without muscles	1	2049	≈ 30	$\approx 5.36e^{-2}$
Tuned with muscles	1	1298	≈ 22	$\approx 7.6e^{-2}$

TABLE I: Required running time for the convergence of the tuned and untuned optimization problem.

The first four muscular constraints (C5-C8) can be interpreted as dynamic constraints acting on each MTU. The final four constraints (C9-C12) ensure that the actual human joint torque is equal to the sum of individual muscle torques. Depending on whether it is an extensor or flexor muscle, the torque is either applied towards the positive or negative direction. Note that since the HAM muscle span both the hip and knee joints, we use $u_m^{(1h)}$ and $u_m^{(1k)}$ to denote the torque HAM has on these two joints respectively. Similarly, we use $u_m^{(4k)}$ and $u_m^{(4a)}$ to denote the knee and ankle joint torques resulting by GAS muscle. The explicit calculation can be found in Eq. 1 with different reference angles in Eq. 2.

Optimization setup. To evaluate our hypothesis that enforcing feasible muscle dynamics would naturally lead to more anthropomorphic behavior, we compare four different gaits generated using FROST [34], for the following variants of the optimization problem:

Name	Included Constraints
Untuned without Muscles	C1-C4
Untuned with Muscles	C1-C12
Tuned without Muscles	Modified C1-C4
Tuned with Muscles	Modified C1-C4, C5-C12

The first two variants compare the framework with and without the inclusion of the muscle models. The final two variants feature modified constraints (C1-C4) in an attempt to achieve the *best* behavior possible as an *expert-tuned* baseline for the *untuned* framework.

These expert-tuned modifications include restricted joint limits based on motion capture data of healthy subject walking from [32], as well as restricted torso movement and joint velocities. A number of foot clearance constraints were

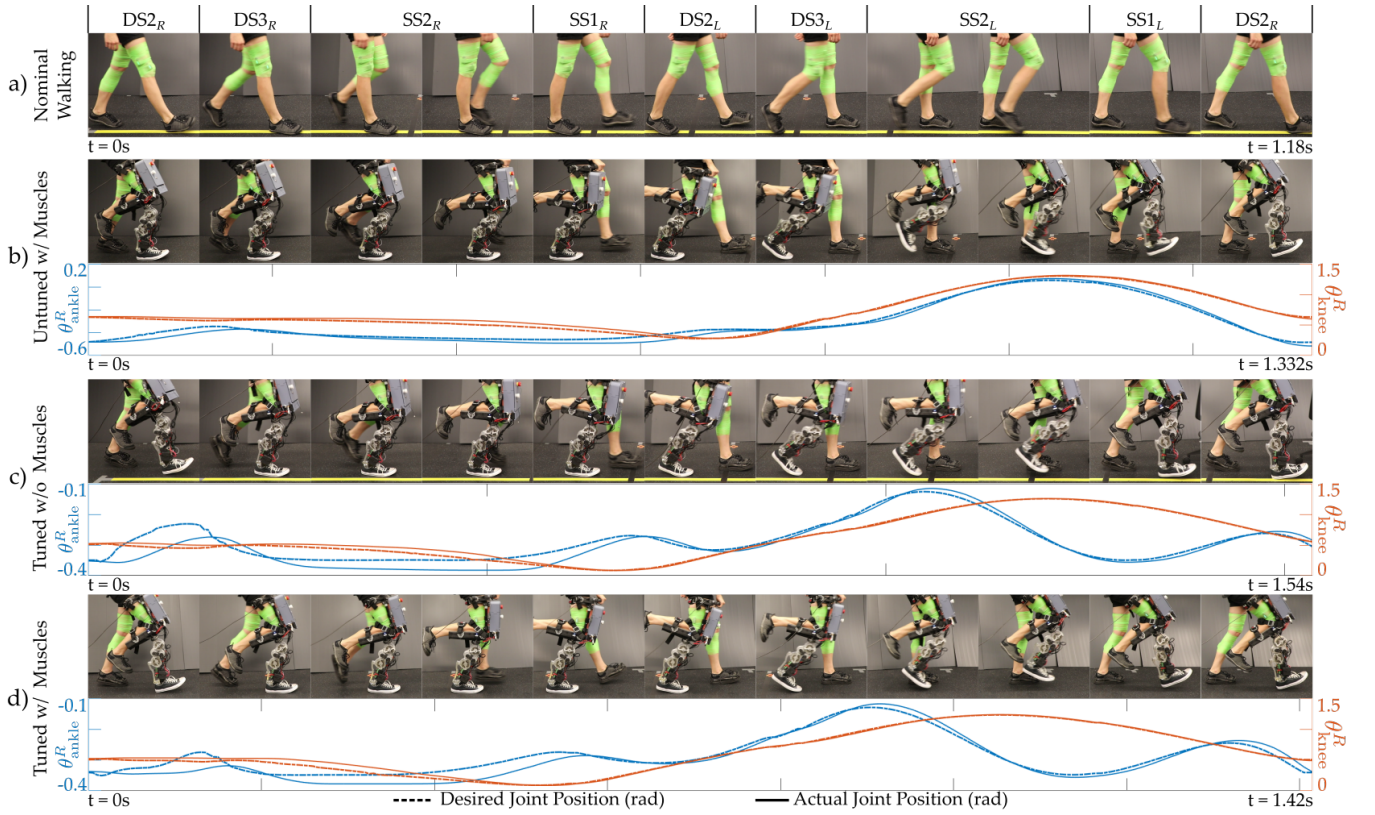


Fig. 7: Gait tiles of experimental demonstration on AMPRO3 for a) normal walking b) untuned with muscles c) tuned without muscles and d) tuned with muscles. The joint tracking across one gait cycle is also plotted below each prosthetic gait.

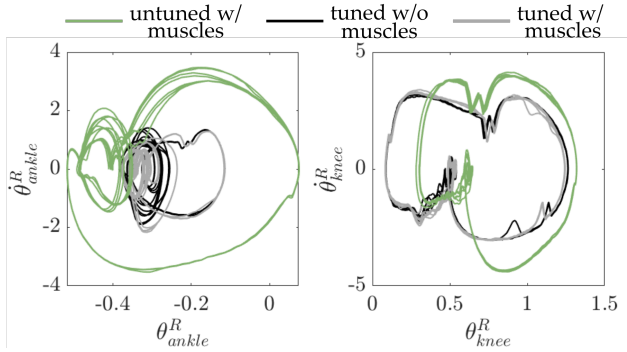


Fig. 8: Limit cycles illustrating the periodic stability achieved during experimental multicontact locomotion (10s of data plotted).

also added to force the swing leg to achieve a desired swing motion. After initial tuning with the optimization parameters, we further shrank HZD-related decision variable constraints (C3) based on preliminary experimental results.

Comparison of generated gaits. We evaluate the performance of our framework in the following two aspects: 1) convergence and associated computation speed, and 2) whether the resulting behavior is anthropomorphic.

Convergence and computation speed. Without any tuning, the nominal HZD optimization problem did not converge, even after running it for 10,000 iterations (~ 10 hours). However, by including the muscle models, the untuned framework was able to converge in approximately 30 minutes (Table. I). For the tuned optimization problems, since the problem is sufficiently constrained after the modification of C1-C4,

the optimization was able to converge in shorter amount of time both with and without the inclusion of muscle models. However, the inclusion of the muscle model comparatively reduced the computation time by approximately 30%, despite adding more decision variables and constraints. We speculate that the muscle model narrows the feasible search space, preventing the solver from aimlessly exploring the high-dimensional search space.

Anthropomorphic behavior. As shown by the simulated gait tiles in Fig. 5a-b, the inclusion of muscle models significantly shapes the generated untuned gait to be different from the nominal version (untuned without muscle). We also notice that the joint trajectories of the untuned gait with muscle models are very similar to normal human joint trajectories (obtained via motion capture (MoCap) in [32]), as shown in Fig. 6. This is striking considering that this behavior is achieved without extensive hand-tuning, which confirmed our assumption that enforcing muscle dynamics did guide the optimization towards generating more nature behavior.

The two tuned gaits yielded nearly identical behavior, reflected by the gait tiles in Fig. 5c-d, and the joint trajectories in Fig. 6a. This is likely because the tuned optimization problem has a small set of feasible solutions. More surprisingly, the behavior of the converged untuned gait is similar to that of the tuned gaits. This highlights the advantage of including muscle models in the gait generation process, as it obviates months of expert tuning. These results preliminarily indicate that our framework is successful at generating stable and natural locomotion.

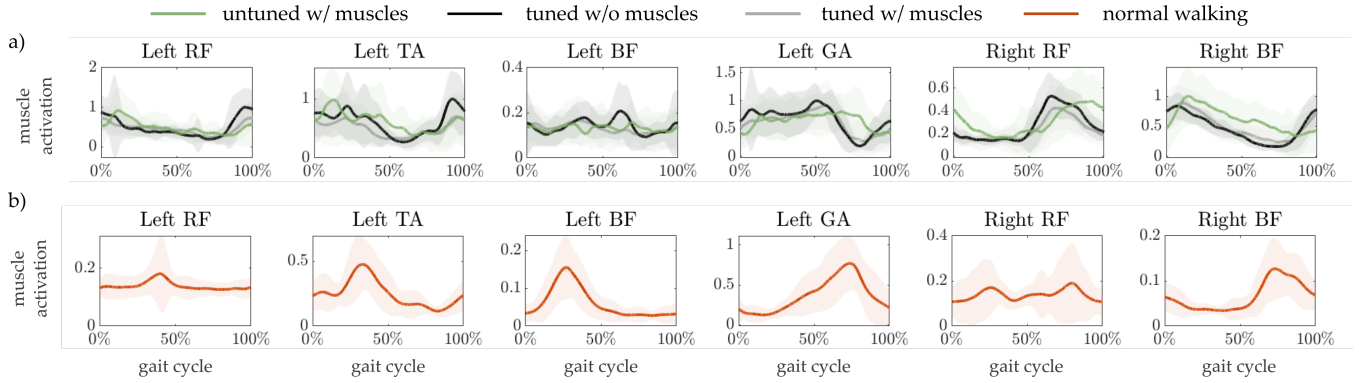


Fig. 9: EMG activity normalized over a full gait cycle for a) prosthetic walking and b) normal walking. All prosthetic walking leads to higher EMG activity, however, the tuned gait with muscles has a slightly less muscle activation compared with the other two gaits.

V. EXPERIMENTAL DEMONSTRATION ON AMPRO3

We experimentally deploy the generated gaits on the dual-actuated transfemoral prosthesis, AMPRO3, with the results highlighted in the supplemental video [35]. During the experiment, a non-disabled human user wore AMPRO3 using an adapter on the right leg as shown in Fig. 1b. The subject was first asked to walk without the prosthesis over a self-selected speed. Then the subject walked with each of the three converged prosthetic gaits. For each gait, the subject was given up to one minute to adjust to the gait before recording the electromyography (EMG) signals. In total, the activity of four muscles on the left leg, including rectus femoris (RF), tibialis anterior (TA), bicep femoris (BF), and gastrocnemius (GAS), and two muscles on the right leg (RF and BF) was recorded with the Trigno wireless biofeedback system (Delsys Inc.), as illustrated in Fig. 1c.

A visualization of the experimental behaviors is provided in Fig. 7 via gait tiles spanning a complete gait cycle (from right heel strike to right heel strike). These gaits were commanded on the prosthetic using a regular joint-level PD controller, with the experimental tracking performance also illustrated in Fig. 7. The stability of the executed gaits is portrayed in Fig. 8 by the periodicity of the limit cycles. It is important to note that achieving this experimentally stable multicontact locomotion is a direct result of leveraging the HZD method to formally generate impact-invariant output trajectories.

As expected, the experimental performance of the tuned gaits was similar. Surprisingly, we observe from the gait tiles that the untuned gait was more aligned with normal walking (in terms of time) than the tuned gait. One speculative explanation for this behavior is that modifying C1-C4 may lead to a less efficient solution due to over-constraining, which is also reflected by a higher objective value of the tuned gaits compared to the untuned gait (Table I).

The average EMG data over one gait cycle for each muscle after preprocessing is shown in Fig. 9. Each of the gaits executed on AMPRO3 yielded similar EMG activity. However, the tuned gait with muscles led to *slightly* less muscle activation than the other two (Fig. 9a). When compared to normal EMG activity (Fig. 9b), we observe that all prosthetic gaits yielded higher muscle activity, which

could be caused by factors such as the extra weight of the prosthesis, different thigh lengths, coordination between the human and the prosthesis. However, when actually designing gaits for an amputee user, the human-prosthesis system would be symmetric, which would likely to result in more natural muscle activation.

VI. CONCLUSION

This work demonstrates the first formal synthesis of stable multicontact locomotion using musculoskeletal models. Specifically, we directly enforce muscle dynamics in the HZD framework to experimentally realize both stable and natural robotic-assisted locomotion on the dual-actuated prosthesis AMPRO3 with a non-disabled human user. We find that incorporating the muscle model guides the optimization problem towards uncovering periodic orbits that resemble natural bipedal locomotion, obviating the need to hand-tune optimization constraints.

Our proposed framework is advantageous since it results in faster computation speeds and less required tuning as compared to state-of-the-art. Additionally, it can be applied to a wide range of behaviors and/or robotic platforms, without relying on the availability of experimental data from human subjects or human-in-the-loop testing.

Future work includes tuning the physiological parameters of the muscle model to account for individual differences and improve the prediction accuracy of the embedded muscle models, using methods similar to those in [36]. Such prediction accuracy would further allow for targeted muscle behavior of the human user for rehabilitation applications.

REFERENCES

- [1] D. A. Winter, *Biomechanics and motor control of human movement*. John Wiley & Sons, 2009.
- [2] S. Kajita, F. Kanehiro, K. Kaneko, K. Fujiwara, K. Yokoi, and H. Hirukawa, "A realtime pattern generator for biped walking," in *Proceedings 2002 IEEE International Conference on Robotics and Automation (Cat. No. 02CH37292)*, IEEE, vol. 1, 2002, pp. 31–37.
- [3] K. Erbaturo and O. Kurt, "Natural zmp trajectories for biped robot reference generation," *IEEE Transactions on Industrial Electronics*, vol. 56, no. 3, pp. 835–845, 2008.
- [4] S. Rezazadeh and J. W. Hurst, "Toward step-by-step synthesis of stable gaits for underactuated compliant legged robots," in *2015 IEEE International Conference on Robotics and Automation (ICRA)*, IEEE, 2015, pp. 4532–4538.

- [5] A. Hereid, S. Kolathaya, M. S. Jones, J. Van Why, J. W. Hurst, and A. D. Ames, "Dynamic multi-domain bipedal walking with atriass through slip based human-inspired control," in *Proceedings of the 17th international conference on Hybrid systems: computation and control*, 2014, pp. 263–272.
- [6] J. Reher, E. A. Cousineau, A. Hereid, C. M. Hubicki, and A. D. Ames, "Realizing dynamic and efficient bipedal locomotion on the humanoid robot durus," in *2016 IEEE International Conference on Robotics and Automation (ICRA)*, IEEE, 2016, pp. 1794–1801.
- [7] M. J. Powell, E. A. Cousineau, and A. D. Ames, "Model predictive control of underactuated bipedal robotic walking," in *2015 IEEE International Conference on Robotics and Automation (ICRA)*, IEEE, 2015, pp. 5121–5126.
- [8] N. Kohl and P. Stone, "Policy gradient reinforcement learning for fast quadrupedal locomotion," in *IEEE International Conference on Robotics and Automation, 2004. Proceedings. ICRA'04. 2004*, IEEE, vol. 3, 2004, pp. 2619–2624.
- [9] H. Benbrahim and J. A. Franklin, "Biped dynamic walking using reinforcement learning," *Robotics and Autonomous Systems*, vol. 22, no. 3–4, pp. 283–302, 1997.
- [10] J. W. Grizzle, G. Abba, and F. Plestan, "Asymptotically stable walking for biped robots: Analysis via systems with impulse effects," *IEEE Transactions on automatic control*, vol. 46, no. 1, pp. 51–64, 2001.
- [11] E. R. Westervelt, J. W. Grizzle, and D. E. Koditschek, "Hybrid zero dynamics of planar biped walkers," *IEEE transactions on automatic control*, vol. 48, no. 1, pp. 42–56, 2003.
- [12] A. D. Ames, K. Galloway, K. Sreenath, and J. W. Grizzle, "Rapidly exponentially stabilizing control lyapunov functions and hybrid zero dynamics," *IEEE Transactions on Automatic Control*, vol. 59, no. 4, pp. 876–891, 2014.
- [13] A. D. Ames, E. A. Cousineau, and M. J. Powell, "Dynamically stable bipedal robotic walking with nao via human-inspired hybrid zero dynamics," in *Proceedings of the 15th ACM international conference on Hybrid Systems: Computation and Control*, 2012, pp. 135–144.
- [14] W.-L. Ma, K. A. Hamed, and A. D. Ames, "First steps towards full model based motion planning and control of quadrupeds: A hybrid zero dynamics approach," in *2019 IEEE/RSJ International Conference on Intelligent Robots and Systems (IROS)*, IEEE, 2019, pp. 5498–5503.
- [15] W.-L. Ma, S. Kolathaya, E. R. Ambrose, C. M. Hubicki, and A. D. Ames, "Bipedal robotic running with durus-2d: Bridging the gap between theory and experiment," in *Proceedings of the 20th international conference on hybrid systems: computation and control*, 2017, pp. 265–274.
- [16] J. P. Reher, A. Hereid, S. Kolathaya, C. M. Hubicki, and A. D. Ames, "Algorithmic foundations of realizing multi-contact locomotion on the humanoid robot durus," *Proc. 12th Adv. Robot. Algorithmic Found. Robot*, vol. 13, pp. 400–415, 2020.
- [17] H. Zhao, J. Horn, J. Reher, V. Paredes, and A. D. Ames, "A hybrid systems and optimization-based control approach to realizing multi-contact locomotion on transfemoral prostheses," in *2015 54th IEEE Conference on Decision and Control (CDC)*, IEEE, 2015, pp. 1607–1612.
- [18] A. D. Ames, "Human-inspired control of bipedal walking robots," *IEEE Transactions on Automatic Control*, vol. 59, no. 5, pp. 1115–1130, 2014.
- [19] J. Zhang, P. Fiers, K. A. Witte, R. W. Jackson, K. L. Poggensee, C. G. Atkeson, and S. H. Collins, "Human-in-the-loop optimization of exoskeleton assistance during walking," *Science*, vol. 356, no. 6344, pp. 1280–1284, 2017.
- [20] H. Han, W. Wang, F. Zhang, X. Li, J. Chen, J. Han, and J. Zhang, "Selection of muscle-activity-based cost function in human-in-the-loop optimization of multi-gait ankle exoskeleton assistance," *IEEE Transactions on Neural Systems and Rehabilitation Engineering*, vol. 29, pp. 944–952, 2021.
- [21] P. K. Jamwal, S. Hussain, Y. H. Tsoi, and S. Q. Xie, "Musculoskeletal model for path generation and modification of an ankle rehabilitation robot," *IEEE Transactions on Human-Machine Systems*, vol. 50, no. 5, pp. 373–383, 2020.
- [22] M. F. Eilenberg, H. Geyer, and H. Herr, "Control of a powered ankle-foot prosthesis based on a neuromuscular model," *IEEE transactions on neural systems and rehabilitation engineering*, vol. 18, no. 2, pp. 164–173, 2010.
- [23] R. L. Waters and S. Mulroy, "The energy expenditure of normal and pathologic gait," *Gait & posture*, vol. 9, no. 3, pp. 207–231, 1999.
- [24] A. V. Hill, "The heat of shortening and the dynamic constants of muscle," *Proceedings of the Royal Society of London. Series B-Biological Sciences*, vol. 126, no. 843, pp. 136–195, 1938.
- [25] H. Geyer, A. Seyfarth, and R. Blickhan, "Positive force feedback in bouncing gaits?" *Proceedings of the Royal Society of London. Series B: Biological Sciences*, vol. 270, no. 1529, pp. 2173–2183, 2003.
- [26] H. Geyer and H. Herr, "A muscle-reflex model that encodes principles of legged mechanics produces human walking dynamics and muscle activities," *IEEE Transactions on neural systems and rehabilitation engineering*, vol. 18, no. 3, pp. 263–273, 2010.
- [27] H. Zhao, A. Hereid, E. Ambrose, and A. D. Ames, "3d multi-contact gait design for prostheses: Hybrid system models, virtual constraints and two-step direct collocation," in *2016 IEEE 55th Conference on Decision and Control (CDC)*, IEEE, 2016, pp. 3668–3674.
- [28] H. Zhao, A. Hereid, W.-l. Ma, and A. D. Ames, "Multi-contact bipedal robotic locomotion," *Robotica*, vol. 35, no. 5, pp. 1072–1106, 2017.
- [29] H. Zhao, E. Ambrose, and A. D. Ames, "Preliminary results on energy efficient 3d prosthetic walking with a powered compliant transfemoral prosthesis," in *2017 IEEE International Conference on Robotics and Automation (ICRA)*, IEEE, 2017, pp. 1140–1147.
- [30] J. W. Grizzle, C. Chevallereau, R. W. Sinnet, and A. D. Ames, "Models, feedback control, and open problems of 3d bipedal robotic walking," *Automatica*, vol. 50, no. 8, pp. 1955–1988, 2014.
- [31] A. D. Ames, R. Vasudevan, and R. Bajcsy, "Human-data based cost of bipedal robotic walking," in *Proceedings of the 14th international conference on Hybrid systems: computation and control*, 2011, pp. 153–162.
- [32] J. Camargo, A. Ramanathan, W. Flanagan, and A. Young, "A comprehensive, open-source dataset of lower limb biomechanics in multiple conditions of stairs, ramps, and level-ground ambulation and transitions," *Journal of Biomechanics*, vol. 119, p. 110320, 2021.
- [33] A. Hereid, E. A. Cousineau, C. M. Hubicki, and A. D. Ames, "3d dynamic walking with underactuated humanoid robots: A direct collocation framework for optimizing hybrid zero dynamics," in *2016 IEEE International Conference on Robotics and Automation (ICRA)*, IEEE, 2016, pp. 1447–1454.
- [34] A. Hereid and A. D. Ames, "Frost*: Fast robot optimization and simulation toolkit," in *2017 IEEE/RSJ International Conference on Intelligent Robots and Systems (IROS)*, IEEE, 2017, pp. 719–726.
- [35] Video of the experimental results. <https://youtu.be/gNL0cG1zqS4>.
- [36] N. Thatte, H. Duan, and H. Geyer, "A method for online optimization of lower limb assistive devices with high dimensional parameter spaces," in *2018 IEEE International Conference on Robotics and Automation (ICRA)*, IEEE, 2018, pp. 5380–5385.